Correlation between Keyhole Geometry and Reflected Laser Light Distribution in Laser-based Manufacturing

Wenkang Huang[1], David Deisenroth[2,*], Sergey Mekhontsev[2], Wenda Tan[1,**]

1 Department of Mechanical Engineering, University of Michigan, Ann Arbor, MI 48109

2 National Institute of Standards and Technology, 100 Bureau Dr. MS 8220, Gaithersburg, MD 20899

* Corresponding author 1: david.deisenroth@nist.gov

** Corresponding author 2: wendatan@umich.edu

Abstract

This study investigated the correlation between the keyhole geometry and reflected laser light distribution during laser-based manufacturing processes. An "imaging dome" system was developed to capture the distribution of the reflected laser light on a registration dome during the process, and found that the reflected laser distribution varied significantly as the keyhole shape was changed by reducing the laser scanning speed. A numerical model was leveraged to understand the multiple reflections of laser rays within the keyholes of different geometries. The results demonstrated the potential of a novel approach for in-situ detection of keyhole shapes during laser-based manufacturing.

Keywords

Laser-based manufacturing, reflected laser light distribution, keyhole geometry, imaging dome, computational physics modeling.

1. Introduction

Keyhole geometry has a significant effect on multiple reflections of laser light in the keyhole during laser-based manufacturing processes, which further affects the laser power absorption into the keyhole and keyhole geometry. Numerous experimental works have been reported to measure the laser energy absorption during laser-based manufacturing processes using calorimetry and integrating sphere methods. The calorimetry method derives the laser energy absorbed by the substrate by measuring the heat exchange between the substrate and a calibrated object, i.e., the calorimeter. The calorimetry method measures the temperature rise of the sample and relates it to the total absorbed laser energy. It can be used to calculate the average absorptivity over a definite time duration [1], [2]. The integration sphere method collects and measures all off-axis light scattered from laser illumination at any moment, and then calculates the instantaneous absorptivity [3]. This method has been combined with inline coherent imaging [4] and synchrotron X-ray imaging [5], [6] techniques to correlate the instantaneous absorptivity with the transient keyhole geometry. Both methods have confirmed the significant rise of laser absorptivity with the formation and growth of keyholes in laser welding and additive manufacturing processes.

As laser absorptivity has been measured as a single-value variable in all these studies, it does not contain rich information about keyhole geometry. It is therefore highly informative to measure the directional distribution of the laser reflection during the process, with the intention of gaining more information about the keyhole shape and behavior. An early work by Mehmetli et al. [7] used a pyroelectric detector to measure the reflected laser radiation at prespecified locations that define a hemisphere on top of the weld spot, and then reconstructed the spatial distribution of a reflected laser beam by combining the measurements at all those locations. In this work, a novel "imaging dome" experimental system was developed for laser-based manufacturing processes to enable in-situ measurement of the directional distribution of reflected laser light as a function of time. The measurement results provided meaningful information regarding the three-dimensional shape of the keyhole. In addition, a computational physics model was used to reproduce the experimental results and understand the correlation between reflected laser light distribution and keyhole geometry.

2. Methodology

Fig. 1 shows the schematic of the imaging dome system developed at the National Institute of Standards and Technology. For a laser remelting process to be studied in this work, an Inconel 718 plate sample was placed at the center of a hemispherical grey registration dome. The reflectivity of the dome was measured to be ~11 % at the laser wavelength of 1070 nm using the facility described in [8]. This relatively low reflectivity value reflects a sufficient amount of light for imaging the first reflection of the laser pattern from the dome but minimizes the integration of light within the hemispherical enclosure. The dome had a radius of 124 mm and was filled with argon gas at atmospheric pressure and room temperature. A laser beam was passed through the inlet port to perform a line scan on the sample along the +X direction. The fiber laser had a spot size of 77 µm with a Gaussian distribution. An equiangular fisheye lens transformed the three-dimensional hemispherical distribution onto the two-dimensional focal plane array (camera chip) such that the zenith angle is proportional to the radial distance from the center of the image (Fig. 1c). As the lens was offset from the center of the hemisphere, the imaging results appeared asymmetric about the X-axis – this problem will be corrected in future work. It should be noted that this metrology uses a similar measurement approach to at least one existing commercial product [11], but is specialized for the conditions of laser-based manufacturing. A parametric study with a constant laser power (285 W) and different scanning speeds (2000 mm/s, 960 mm/s, and 500 mm/s) was performed to produce keyholes of different shapes.

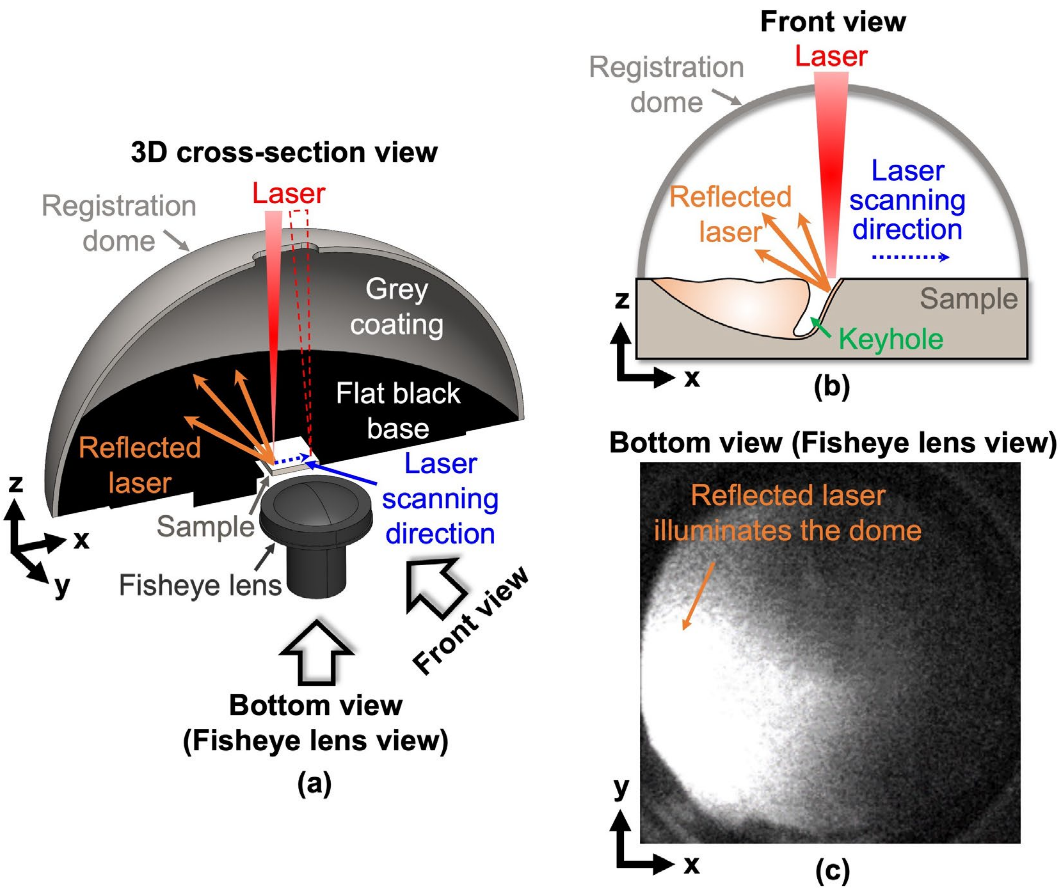

Fig. 1. (a) Three-dimensional cross-section view of the imaging dome system, (b) schematic of the front view of the system, and (c) experimental results of the bottom view (Fisheye lens view) image of the registration dome in laser-based manufacturing processes.

On the modeling side, a three-dimensional computational physics model developed at the University of Michigan was used to simulate the experiments [[11], [12], [13], [10]]. The model takes the processing parameters (scanning speed, laser power, laser spot size, power distribution profile) and temperature-dependent material properties as inputs [[14], [15]]. It solves the conservation equations of mass, momentum, and energy to predict the pressure, velocity, and temperature fields in the molten pool. It also solves the level-set equation to track the dynamic keyhole evolution. A ray-tracing model has been incorporated to capture the multiple reflections and absorption of the laser in the keyhole.

3. Results and discussion

With the decreasing scanning speed in cases (a)–(c), the fusion zone became deeper (Fig. 2), suggesting increasing keyhole depths caused by the increase of laser heat input. This variation trend was captured by the simulations. Admittedly the simulations did not exactly reproduce the keyhole shapes in different cases, which was attributed to the insufficient calibration of the material properties in the model.

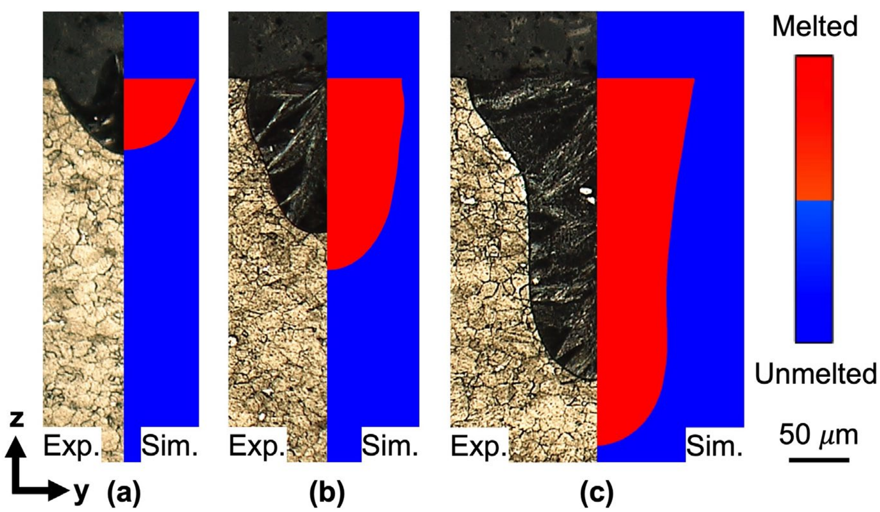

Fig. 2. Comparison of experimental and simulation results of fusion zone geometries for the three cases with laser power of 285 W and scanning speed of (a) 2000 mm/s, (b) 960 mm/s, and (c) 500 mm/s.

The reflected laser light distribution on the dome changed accordingly (Fig. 3). Bright spots due to the reflected laser light were found on the dome in cases (a) and (b), as marked by the red dashed lines in Fig. 3. With the decrease of the scan speed, the bright spot moved from the negative end on the X-axis (which is located behind the keyhole and molten pool) toward the center of the dome (which is located on top of the keyhole and molten pool), and became less spanned along the Y-axis (i.e. the transverse direction). The reflected laser light appeared more evenly distributed over the entire dome in case (c).

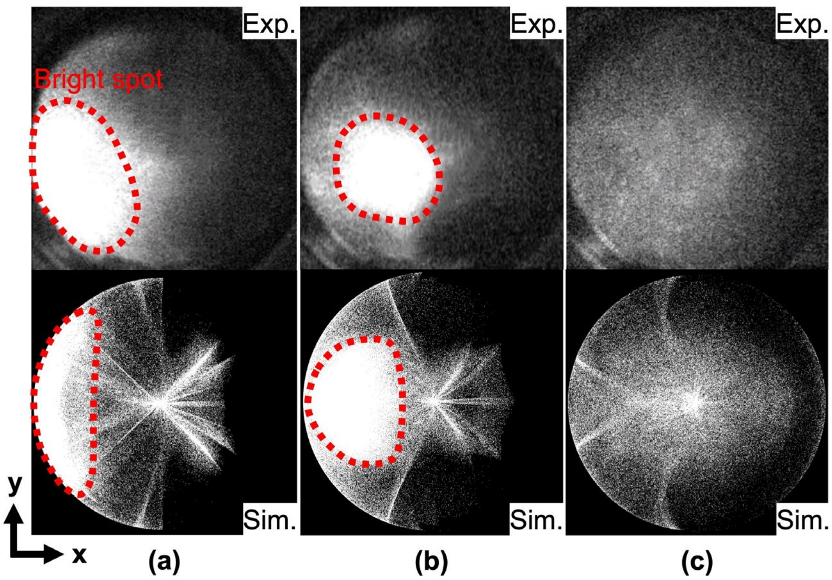

Fig. 3. Comparison of experimental and simulation results of reflected laser light distributions on registration dome for the three cases with laser power of 285 W and scanning speed of (a) 2000 mm/s, (b) 960 mm/s, and (c) 500 mm/s. Imaging frequency for experimental results was 10 kHz.

The simulation results in Fig. 4 explained the translation of the bright spots along X-axis due to the variation of keyhole shape from the side views. The keyhole in case (a) was long (on the X axis) and shallow (on the Z axis). The traveling route of one typical ray in this keyhole was shown in Fig. 4a by a series of arrows, each showing one time of reflection. The rays usually left the keyhole along the −X direction with a small velocity component along the +Z direction (i.e., slightly upward). These rays ultimately registered on the dome on the far end along the −X direction, generating the bright spot at the end of the −X axis. The keyhole became deeper and shorter in case (b). The laser rays, as shown by the red arrows in Fig. 4b, typically left the keyhole with a reduced velocity component along the −X direction and an increased component along the +Z direction. Most rays illuminated the dome at locations closer to its top, causing the bright spot to shift toward the dome center. The keyhole became even deeper in case (c), and the keyhole length (on the X axis) was further reduced to be comparable with the keyhole width (on the Y axis). The laser rays were reflected between the walls in all directions of this deep and slender keyhole, with one example shown by the red arrows in Fig. 4c. Due to the irregular shape of the keyhole, the rays had arbitrary paths, and ultimately left the keyhole with random paths, illuminating the dome in a fairly uniform manner.

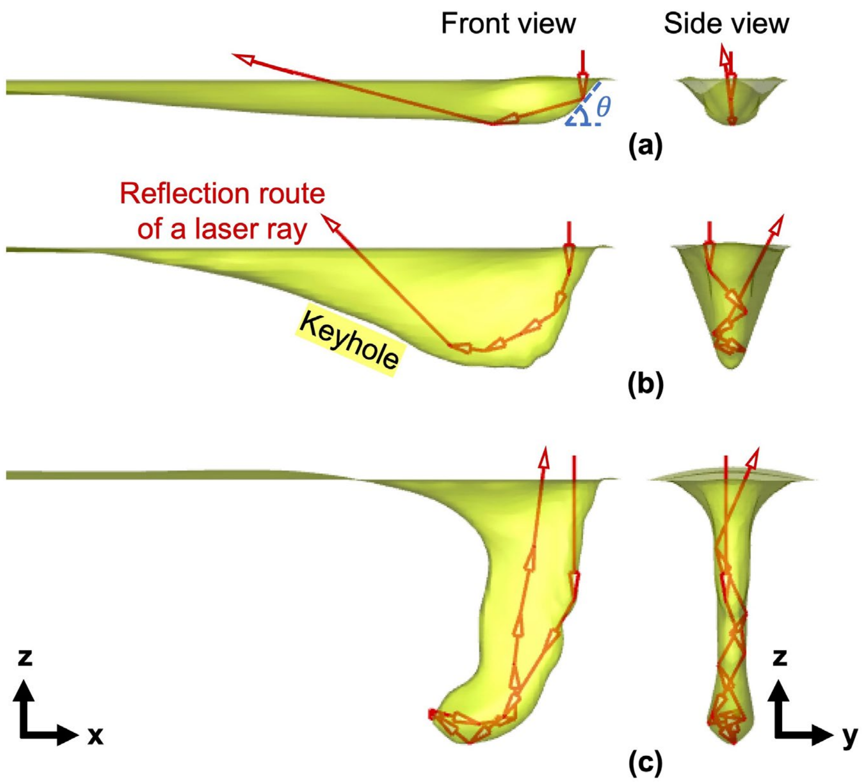

Fig. 4. Simulation results of the front view and side view of keyhole and a typical laser ray multiple-reflection route in the keyhole for the three cases with laser power of 285 W and scanning speed of (a) 2000 mm/s, (b) 960 mm/s, and (c) 500 mm/s.

Similarly, the reduced span of the bright spots on the Y axis could be explained by the variation of keyhole shape from the front view. The keyhole in case (a) was shallow on its cross-section (front view of Fig. 4a), allowing the reflected ray to leave the cavity with rather large divergence angles and thus illuminate the registration dome over a large span on the Y-axis. The keyhole in case (b) became deeper, which limited the divergence angle of the escaped rays and hence the transverse span of the bright spot on the registration dome. In case (c), the reflected rays left the keyhole in random directions, and no bright spot was found on the dome.

4. Summary and Future Work

In this work, an imaging dome system was developed to capture the temporal directional distributions of the reflected laser light by a keyhole in laser-based manufacturing processes, and a computational physics model was leveraged to predict the keyhole shape and reveal the routes of multiple reflections of the rays in the keyhole. The work demonstrated the correlation between the keyhole shape and the reflected laser light distribution, which can be used as a new approach for in-situ detection of keyhole shape during laser-based manufacturing. Future work has been planned to improve the measurement capabilities. Further characterization of imaging quality, artifacts, and distortions can improve the quantitative accuracy of the image data. Photodiodes with high collection angles may be included to measure the total reflected laser power. The computational physics model will be further calibrated for IN718 to enable better predictions of the keyhole and molten pool shapes. Statistical analyses should be performed for the experimental and simulation data to identify more quantitative correlations between keyhole shape and reflected laser light distribution, and the simulation results should be further leveraged to understand the correlations.

Data Availability

The raw/processed data required to reproduce these findings cannot be shared at this time as the data also forms part of an ongoing study.

Acknowledgments

WH and WT wish to gratefully acknowledge the financial support provided by the National Science Foundation under Grant No. 2223007. DD wishes to thank Alexander M. Rubenchik for thoughtful discussions that inspired the development of the described metrology.

References

[1] Kim TH, Charles, Albright E, Chiang S, Albright CE, Kim P. The Energy Transfer Efficiency in Laser Welding Process. J Laser Appl 1990;2:23–8. https://doi.org/10.2351/1.4745249.

[2] Trapp J, Rubenchik AM, Guss G, Matthews MJ. In situ absorptivity measurements of metallic powders during laser powder-bed fusion additive manufacturing. Appl Mater Today 2017;9:341–9. https://doi.org/10.1016/J.APMT.2017.08.006.

[3] Fabbro R, Bermejo D, Orza J, Sabatier L, Leprince L, Remy Fabbro, et al. Absorption measurements in continuous high-power CO2 laser processing of materials. Https://DoiOrg/101117/1220566 1990;1276:461–7. https://doi.org/10.1117/12.20566.

[4] Allen TR, Huang W, Tanner JR, Tan W, Fraser JM, Simonds BJ. Energy coupling mechanisms revealed through simultaneous keyhole depth and absorptance

measurements during laser-metal processing. Phys Rev Appl 2020;13:. https://doi.org/10.1103/PhysRevApplied.13.064070064070.

[5] Simonds BJ, Tanner J, Artusio-Glimpse A, Williams PA, Parab N, Zhao C, et al. The causal relationship between melt pool geometry and energy absorption measured in real time during laser-based manufacturing. Appl Mater Today 2021;23:101049. , https://doi.org/10.1016/J.APMT.2021.101049.

[6] Khairallah SA, Sun T, Simonds BJ. Onset of periodic oscillations as a precursor of a transition to pore-generating turbulence in laser melting. Additive Manufacturing Letters 2021;1:100002. https://doi.org/10.1016/j.addlet.2021.100002.

[7] Mehmetli BA, Takahashi K, Sato Shunichi. Direct measurement of reflectance from aluminum alloys during CO2 laser welding. Applied Optics, Vol 35, Issue 18, Pp 3237-3242 1996;35:3237–42. https://doi.org/10.1364/AO.35.003237.

[8] Hanssen LM, Kaplan S. Infrared diffuse reflectance instrumentation and standards at NIST. Anal Chim Acta 1999;380:289–302. , https://tsapps.nist.gov/publication/get_pdf.cfm?pub_id=103848.

[9] Kostal H, Kreysar D, Rykowski R. Application of Imaging Sphere for BSDF Measurements of Arbitrary Materials. Frontiers in Optics 2008/Laser Science XXIV/Plasmonics and Metamaterials/Optical Fabrication and Testing (2008), Paper FMJ6 2008:FMJ6. https://doi.org/10.1364/FIO.2008.FMJ6.

[10] Tan W, Huang W. Numerical modeling of thermo-fluid flow and metal mixing in laser keyhole welding of dissimilar metals. ASME 2018;V002T04A043.(2). https://doi.org/10.1115/MSEC2018-6640.

[11] Li X, Zhao C, Sun T, Tan W. Revealing Transient Powder-Gas Interaction in Laser Powder Bed Fusion Process through Multi-physics Modeling and Highspeed Synchrotron X-ray Imaging. Addit Manuf 2020:101362. https://doi.org/ 10.1016/j.addma.2020.101362.

[12] Li X, Guo Q, Chen L, Tan W. Quantitative investigation of gas flow, powder-gas interaction, and powder behavior under different ambient pressure levels in laser powder bed fusion. Int J Mach Tools Manuf 2021;170:103797. , https://doi.org/10.1016/J.IJMACHTOOLS.2021.103797.

[13] Kouraytem N, Li X, Cunningham R, Zhao C, Parab N, Sun T, et al. Effect of lasermatter interaction on molten pool flow and keyhole dynamics. Physical Review Applied 2019;11(6):. , https://doi.org/10.1103/PhysRevApplied.11. 064054064054.

[14] Hosaeus H, Seifter A, Kaschnitz E, Pottlacher G. Thermophysical properties of solid and liquid inconel 718 alloy. High Temp High Press 2001;33:405–10. , https://citeseerx.ist.psu.edu/document?repid=rep1&type=pdf&doi= 3cfe53e3a1212efd66eca53a87e37774fa5ba49e.

[15] Pottlacher G, Hosaeus H, Kaschnitz E. Seifter A Thermophysical properties of solid and liquid Inconel 718 Alloy. Scandinavian Journal of Metallurgy 2002;31:161–8. https://doi.org/10.1034/j.1600-0692.2002.310301.x.